Nanoscale

ROYAL SOCIETY OF CHEMISTRY

PAPER

View Article Online
View Journal | View Issue

Open Access Article. Published on 23 December 2021. Downloaded on 1/20/2026 12:19:44 PM.
This article is licensed under a Creative Commons Attribution-NonCommercial 3.0 Unported Licence.

Check for updates

Cite this: *Nanoscale*, 2022, **14**, 1767

Metallo-boranes: a class of unconventional superhalogens defying electron counting rules†

Huta Banjade, Hong Fang and Puru Jena *

Superhalogens are a class of highly electronegative atomic clusters whose electron affinities exceed those of halogens. Due to their potential for promoting unusual reactions and role as weakly coordinating anions as well as building blocks of bulk materials, there has been considerable interest in their design and synthesis. Conventional superhalogens are composed of a metal atom surrounded by halogen atoms. Their large electron affinities are due to the fact that the added electron is distributed over all the halogen atoms, reducing electron–electron repulsion. Here, using density functional theory with a hybrid exchange–correlation functional, we show that a new class of superhalogens can be developed by doping *closo*-boranes (*e.g.*, $B_{12}H_{12}$) with selected metal atoms such as Zn and Al as well as by replacing a B atom with Be or C. Strikingly, these clusters defy electron counting rules. For example, according to the Wade–Mingos rule, $Zn(B_{12}H_{12})$ and $Al(BeB_{11}H_{12})$ are closed-shell systems that should be chemically inert and, hence, should have very small electron affinities. Similarly, $Zn(B_{12}H_{11})$, $Al(B_{12}H_{12})$, and $Zn(CB_{11}H_{12})$, with one electron more than needed for electronic shell closure, should behave like superalkalis. Yet, all these clusters are superhalogens. This unexpected behavior originates from an entirely different mechanism where the added electron resides on the doped metal atom that is positively charged due to electron transfer.

Received 19th October 2021,
Accepted 22nd December 2021

DOI: 10.1039/d1nr06929b

rsc.li/nanoscale

1. Introduction

One of the important concepts that has emerged in cluster science is that of superatoms,[1] which are atomic clusters of given size and composition mimicking the chemistry of elements in the periodic table. Superhalogens[2] and superalkalis[3] are superatoms that mimic the chemistry of halogen and alkali atoms, respectively. The former have electron affinities (EA) *larger* than those of halogens, while the latter have vertical ionization energies (VIE) *smaller* than those of alkali atoms. EA is defined as the energy difference between the anion and the neutral cluster, both in their respective ground state configurations. VIE, on the other hand, is the energy difference between the neutral and positively charged cluster, both at the ground state geometry of the neutral. The highest electron affinity of a halogen atom is that of Cl, namely 3.6 eV, and the lowest ionization energy of an alkali atom is that of Cs, namely 3.89 eV. While early works on superhalogens and superalkalis were of academic interest, it has now been shown that these species can be used to form new supersalts[4] with unique properties. For example, superhalogens and hyperhalogens[5] (clusters with EAs even larger than those of superhalogens) can serve as the building blocks of hydrogen storage materials,[6] halogen-free electrolytes in metal-ion batteries,[7] hybrid perovskite solar cells resistant to moisture,[8] and ion conductors with enhanced ionic conductivities.[9] It has also been shown that superhalogens can be used in the design of multiferroic materials.[10] These promising technological applications have led to a surge of research in identifying novel superhalogen moieties.

According to the original design by Gutsev and Boldyrev,[2] superhalogens[11–15] with composition MX_{k+1} are composed of a metal atom (M) and $k + 1$ halogen atoms (X), where k is the maximal valence of the metal atom. The design principle has been based on the octet electron-counting rule[16] for low atomic number species and the 18-electron rule[17] for transition metals. In the former, outer s and p orbitals are filled with 2 and 6 electrons, while in the later s, p, and d orbitals are filled with 2, 6, and 10 electrons, respectively. Typical examples of superhalogens containing transition metal atoms include $M@Au_{12}$ (M = V, Nb, Ta).[18] In addition, there are superhalogens, such as H_nF_{n+1},[19] that do not contain any metal atom and MH_n[20] (M being a non-transition metal element like Be, Mg, Al) that do not contain any halogen atom. The high EA of these superhalogens is due to the added electron being shared by multiple halogen atoms in the cluster, leading to reduced electron–electron repulsion. For nearly three decades since the prediction of superhalogens, the design and synthesis of these species fol-

Physics Department, Virginia Commonwealth University, Richmond, VA 23284, USA. E-mail: pjena@vcu.edu

†Electronic supplementary information (ESI) available. See DOI: 10.1039/d1nr06929b

Open Access Article. Published on 23 December 2021. Downloaded on 1/20/2026 12:19:44 PM.
This article is licensed under a Creative Commons Attribution-NonCommercial 3.0 Unported Licence.

lowed the above Gutsev-Boldyrev strategy. Later, Jena and co-workers showed that electron counting rules such as the Wade–Mingos rule[21] and Huckel's rule[22,23] could also be used to design superhalogens composed of borane-based clusters[24,25] and organic molecules,[26] respectively. It was also shown that the electron affinity of superhalogens can be further increased by simultaneously satisfying multiple electron-counting rules.[27,28] All these species can be classified as "conventional" superhalogens.

In this paper, we show that, to create a superhalogen, it is *not* necessary for the added electron to be distributed over the electronegative sites nor for the cluster to follow specific electron counting rules; superhalogens can be created in defiance of the electron shell-closure rule. We demonstrate this by focusing on two types of metallo-boranes; closed-shell metallo-boranes, *e.g.*, $Zn(B_{12}H_{12})$ and $Al(BeB_{11}H_{12})$, and metallo-boranes with one electron more than needed for electron shell closure, *e.g.*, $Zn(B_{12}H_{11})$, $Zn(CB_{11}H_{12})$, and $Al(B_{12}H_{12})$. However, as expected, metallo-boranes with one less electron than needed for shell closure, *e.g.*, $Zn(BeB_{11}H_{12})$ and $Li(B_{12}H_{12})$, are conventional superhalogens. Note that the stability of *closo*-boranes, B_nH_n, is governed by the Wade–Mingos polyhedral skeletal electron pair theory (PSEPT). Here, $(4n + 2)$ electrons are required for electron shell closure, where n is the number of vertices of the boron polyhedron. As B_nH_n clusters have $4n$ electrons, two more are needed for their stability, and $B_nH_n^{2-}$ is a stable cluster. The second electron affinity, *i.e.*, energy gained when the second electron is attached to $B_{12}H_{12}^{-}$, is 0.9 eV.[29,30] Zn, being divalent, can contribute the needed two electrons, and hence $Zn(B_{12}H_{12})$ should form a closed shell cluster according to the Wade–Mingos rule. Similarly, $Al(BeB_{11}H_{12})$ should obey the Wade–Mingos rule as $BeB_{11}H_{12}$ requires three electrons for the electron shell closure, these being supplied by the trivalent Al atom. Consequently, the electron affinities of these clusters are expected to be small, certainly less than those of halogens, as is the case with any closed shell or alkali-like systems. However, our calculations based on density functional theory and hybrid exchange–correlation potential revealed just the opposite. $Zn(B_{12}H_{12})$ and $Al(BeB_{11}H_{12})$ clusters with closed shells as well as $Zn(B_{12}H_{11})$, $Zn(CB_{11}H_{12})$, and $Al(B_{12}H_{12})$ clusters with one electron more than needed for the electron shell closure turn out to be superhalogens – in defiance of the Wade-Minogs rule. Conventional wisdom would have dictated otherwise – the former clusters should have low EAs, while the latter should be superalkalis. The origin of these "unconventional" superhalogens is different; here, the added electron resides on the doped metal atom, which is in a positively charged state due to the transfer of charge to the cluster.

2. Computational method

All calculations are performed using density functional theory[31] with the long-range corrected hybrid exchange–correlation functional ωB97XD[32] and 6-311+g(d,p) basis sets embedded in the Gaussian16 package.[33] The preferred site of the doped metal atom was determined by considering both endohedral and exohedral positions. Geometries are optimized without any symmetry constraint. Default convergence criteria are used for the force (4.5×10^{-4} Hartree per Bohr) and displacement (1.8×10^{-3} Bohr). The output symmetries given in Table S1† are kept at a tolerance of 0.1 Å using the Gaussview. Our previous calculations[34] showed that the EAs and VIEs obtained using the above procedure are accurate to within 0.2 eV compared to the experiment. No imaginary frequency is found for the optimized geometries. VIE, EA, and vertical detachment energy (VDE) are calculated using the total energies of the clusters with different charge states. VDE is the energy difference between the anion and the neutral, both at the ground state geometry of the anion. The difference between EA and VDE, thus, is a measure of the effect of structural relaxation of the anionic cluster when the extra electron is removed. Natural bond orbital analysis (NBO) is performed to study the charge states of the atoms.[35] The nature of bonding between the adsorbed metal atom and the cluster is studied using Bader's Quantum theory of atoms in the molecule (QTAIM)[36] approach. This is illustrated by calculating the contour map of the Laplacian of the electron density[37] using the Multiwfn package.[38] To better understand the electronic structure, we have further calculated the energy gaps between the highest occupied molecular orbital (HOMO) and the lowest unoccupied molecular orbital (LUMO), the projected density of states, and the charge density difference (CDD) of the studied clusters. CDD is obtained by subtracting the superimposed electron density of the selected fragments from the total electron density of the clusters. The projected density of states is obtained by using the C-squared population analysis (SCPA) method proposed by Ros and Schuit[39] as implemented in the Multiwfn package; during this calculation, we have removed the diffuse function. The original discrete molecular orbital energy levels are convoluted with a Gaussian function resulting in a smooth yet broadened DOS, as shown in Fig. 2. With the calculated DOS, our goal is to identify the electronic/elemental compositions of the frontal orbitals. Besides, thermally vibrational stability of the cluster is studied by using AIMD simulation; see ESI† for the details.

3. Results and discussion

In the following, we discuss the equilibrium geometries, electronic structure, nature of bonding, EA, VDE, and VIE of the three types of metallo-borane clusters.

A. Closed-shell metallo-boranes: $Zn(B_{12}H_{12})$ and $Al(BeB_{11}H_{12})$

closo-Dodecaborates and their derivatives, *e.g.*, $B_{12}H_{12}^{2-}$ and $BeB_{11}H_{12}^{3-}$, are very stable clusters that satisfy the Wade–Mingos electron shell closure rule. Here, we consider two clusters $Zn(B_{12}H_{12})$ and $Al(BeB_{11}H_{12})$. Being divalent, Zn is expected to donate the two electrons needed to stabilize $B_{12}H_{12}$, while Al, being trivalent, can donate three electrons to

Open Access Article. Published on 23 December 2021. Downloaded on 1/20/2026 12:19:44 PM.
This article is licensed under a Creative Commons Attribution-NonCommercial 3.0 Unported Licence.

stabilize $BeB_{11}H_{12}$. Thus, both $Zn(B_{12}H_{12})$ and $Al(BeB_{11}H_{12})$ are expected to have closed shells and, therefore, should possess small EAs. To see if this is indeed the case, we first calculated the equilibrium geometries of these clusters. Note that the doped metal atom can occupy either the endohedral or the exohedral site. We have studied both possibilities and found the endohedral site to be unstable. Indeed, both Zn and Al atoms in $Zn(B_{12}H_{12})$ and $Al(BeB_{11}H_{12})$ clusters came out of the cage after optimization. In $Zn(B_{12}H_{12})$, the endohedral site is higher in energy by 2.95 eV. The higher energy isomer of $Zn(B_{12}H_{12})$ is given in Fig. S1(a).† While in $Al(BeB_{11}H_{12})$ the Al atom takes place of the Be atom in $BeB_{11}H_{12}$, independent of whether Al atom is placed in endohedral or exohedral site. This is consistent with the previous study on similar systems.[28] The optimized geometries of neutral and anionic $Zn(B_{12}H_{12})$ are plotted in Fig. 1(a) and (b), respectively. In the neutral cluster, Zn is bonded to three H atoms, two of which are at a distance of 1.90 Å, while the third one is at a marginally shorter distance of 1.89 Å. Zn is equidistant from the three nearest B atoms at 2.12 Å. In the anionic $Zn(B_{12}H_{12})^-$ cluster, the three closest H atoms are at a distance of 2.05 Å, while the three closest B atoms are at a distance of 2.30 Å from Zn. Distortion in the boron cage is found to be small and the B–B bond length forming the triangle below the adsorbed Zn is 1.79 Å, only slightly greater than the others, namely, 1.77 Å. The B–H bond lengths range from 1.19 to 1.23 Å, with the H bonded to Zn having the shortest distance. The addition of electron increases the Zn–H and Zn–B distances to 2.05 and 2.30 Å in the anion compared to 1.89 and 2.12 Å in a neutral state, respectively.

It is interesting to note that Zn–H distance of 1.89 Å is shorter than that of the K–H distance of 2.29 Å in crystalline $K_2(B_{12}H_{12})$.[40] To see if this difference could be due to the fact that our study is based on an isolated cluster while $K_2(B_{12}H_{12})$ is crystalline, we optimized the geometry of $K_2(B_{12}H_{12})$ cluster. The calculated K–H distance of 2.55 Å is larger than that in the crystalline phase. Thus, one would expect that in $Zn(B_{12}H_{12})$ crystal the Zn–H distance would be even smaller than 1.89 Å. The difference between the Zn–H and K–H distance is due to the size effect – the ionic radii of Zn and K are 74 pm and 138 pm, respectively.

The equilibrium geometries of neutral and anionic Al $(BeB_{11}H_{12})$ clusters are given in Fig. 1(c) and (d). It has been shown before that replacing a B atom with Be in the B_{12} icosahedral cage would lead to a stable trianion.[41] Thus, we hypothesized that adding an Al atom to $BeB_{11}H_{12}$ would make a closed-shell stable cluster, yielding a cluster where the Al atom is bound to an unperturbed $BeB_{11}H_{12}$ cage. Geometry optimization, however, led to a different geometry of $Al(BeB_{11}H_{12})$. As seen in Fig. 1(c), the Al atom formed the cage with 11 B atoms, with the Be atom bonded to $AlB_{11}H_{12}$. This structure (Fig. 1(c)) was found to be 2.18 eV lower in energy than the one when Be

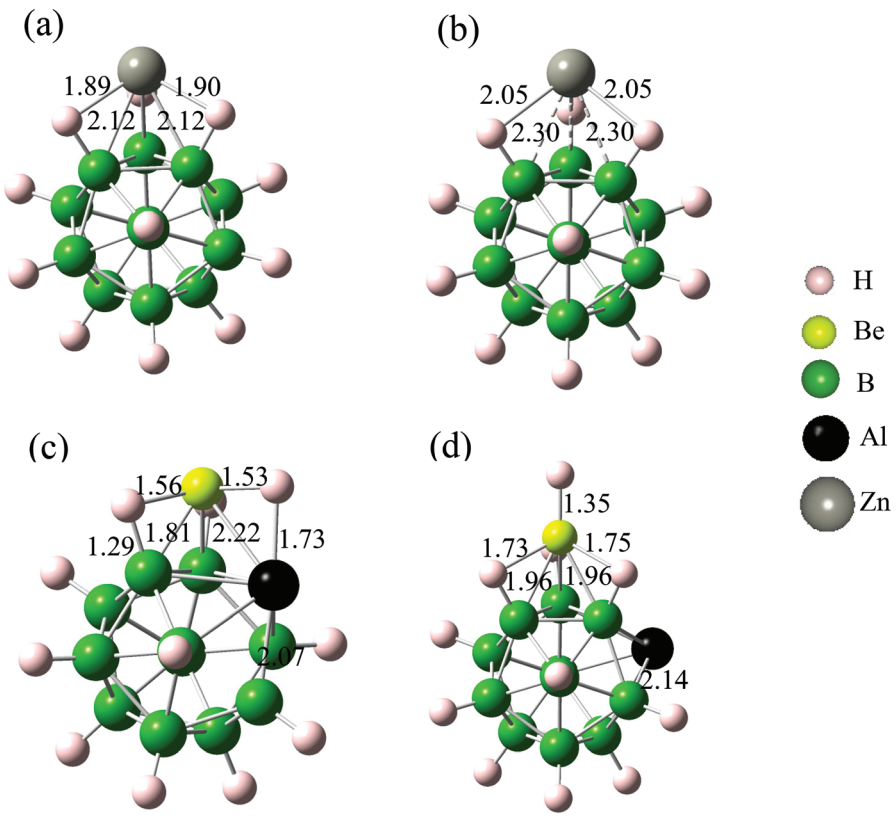

Fig. 1 Optimized geometries of (a) neutral $Zn(B_{12}H_{12})$, (b) anionic $Zn(B_{12}H_{12})$, (c) neutral $Al(BeB_{11}H_{12})$, and (d) anionic $Al(BeB_{11}H_{12})$. The bond lengths (in Å) from Zn in $Zn(B_{12}H_{12})$, and Al, Be in $Al(BeB_{11}H_{12})$ to the nearest atoms in the cluster are shown.

Open Access Article. Published on 23 December 2021. Downloaded on 1/20/2026 12:19:44 PM.
This article is licensed under a Creative Commons Attribution-NonCommercial 3.0 Unported Licence.

forms the cage with the B atoms as shown on Fig. S1(b).† In retrospect, this makes sense as Al is trivalent like B. Be atom is adsorbed at a bridge site between two B atoms, with a B–Be bond length of 1.81 Å. H atom, which was bonded previously with the B atom, is displaced from its original position and aligns at the bridge site between Al and Be, with a bond length of 1.73 and 1.53 Å to Al and Be, respectively. Besides, the Be atom is bonded to two other H atoms at a distance of 1.56 Å. In contrast, the Al–B distance ranges from 2.07 to 2.22 Å, and Al–Be bond distance is 2.22 Å. In $Al(BeB_{11}H_{12})$, some of the Al–B interactions become stronger, while they get weaker in the anion [Fig. 1(d)]. This can be understood by analyzing the Al–B bond distances, namely 2.07–2.22 Å in the neutral *vs.* 2.14–2.18 Å in the anion. In the anionic $Al(BeB_{11}H_{12})$, Be atom lies at a top site of the triangle formed by three B atoms of the cage; it is bonded with four H atoms (Be–H bond distance ranges from 1.35 to 1.75 Å), and three B atoms (Be–B bond distance is 1.95, 1.96, and 1.96 Å).

The EA and VDE of $Zn(B_{12}H_{12})$, presented in Table 1, are 4.30 eV and 4.70 eV, respectively. This small difference is typical in cases where the ground state geometries of the neutral and its anion are not very different. However, the situation is different for $Al(BeB_{11}H_{12})$, where the EA and VDE are 3.61 eV and 4.44 eV, respectively. This large difference of 0.83 eV is a consequence of significant changes in the geometries of the neutral and anionic clusters.

To understand the origin of this behavior, we have analyzed the electronic structure of the neutral and anionic clusters. First, we discuss the charge distribution. In the neutral $Zn(B_{12}H_{12})$ cluster, the charge on the Zn atom is +1.50*e*, as can be seen from Fig. S2(a).† This is consistent with what we had hypothesized earlier, *i.e.*, Zn would donate most of its two electrons to satisfy the charge requirement of $B_{12}H_{12}$, in keeping with the Wade–Mingos rule. Once an extra electron is added, the charge on the Zn site in $Zn(B_{12}H_{12})^-$ decreases to +0.79*e*. This clearly shows that instead of being distributed over the H atoms, the added electron goes to the positively charged Zn site. Note that the ionization energy of the Zn atom is 9.34 eV. Thus, as the added electron goes to the Zn site, it gains energy, not because it is distributed over a large phase space but because it neutralizes the Zn atom. Thus, $Zn(B_{12}H_{12})$ is an unconventional superhalogen and can serve as a model for the design of many such species.

Table 1 Calculated vertical ionization energy (VIE), vertical detachment energy (VDE), electron affinity (EA), and HOMO–LUMO gap (ΔG) of the studied clusters

Cluster	IE (eV)	VDE (eV)	EA (eV)	ΔG (eV)
$Zn(B_{12}H_{12})$	9.73	4.70	4.30	6.0
$Al(BeB_{11}H_{12})$	9.24	4.44	3.61	4.70
$Zn(B_{12}H_{11})$	8.78	4.69	3.93	5.79
$Al(B_{12}H_{12})$	10.12	5.07	4.43	6.21
$Zn(CB_{11}H_{12})$	8.60	5.49	3.68	6.10
$Zn(BeB_{11}H_{12})$	8.32	4.12	3.67	5.73
$Li(B_{12}H_{12})$	9.83	5.90	4.85	5.92

This is also what we see in $Al(BeB_{11}H_{12})$. Here, in the neutral $Al(BeB_{11}H_{12})$ cluster, Al and Be carry charges of +1.4*e* and +1.6*e*, respectively, as they donate the electrons to the cage needed for electronic shell closure. As an extra electron is added, we observe that the charges at the Al and Be sites in $Al(BeB_{11}H_{12})^-$ decrease to +1.19*e* and +1.45*e*, respectively (see Fig. S2(b)†). As the ionization energies of Al and Be atoms are respectively 5.99 eV and 8.83 eV, energy is gained as the added electron partially neutralizes these sites. Consequently, $Al(BeB_{11}H_{12})$ is a superhalogen, although its EA of 3.61 eV is marginally larger than that of Cl, namely, 3.60 eV.

Next, we analyze the electronic structure and bonding characteristics by studying the HOMO–LUMO gap, the partial density of states, the charge density difference, and Bader's quantum theory of atoms in molecules (QTAIM) analysis. The computed HOMO–LUMO gaps of these clusters are shown in Table 1. What is surprising is that both $Zn(B_{12}H_{12})$ and $Al(BeB_{11}H_{12})$ clusters are superhalogens, in spite of being closed-shell systems and having large HOMO–LUMO gaps of 6.0 and 4.7 eV, respectively. HOMO–LUMO gap can be considered as an indicator of electronic stability and chemical reactivity of clusters. Note that the clusters with large HOMO–LUMO gaps are reluctant to donate or accept an electron from a low-lying HOMO or high-lying LUMO. In addition, the change in the gap, with the addition of an electron, can give us some clue about the stability of the anion compared to that of the neutral cluster.

Fig. 2 shows the projected density of states of $Zn(B_{12}H_{12})$ and $Al(BeB_{11}H_{12})$ clusters. Orbital composition analysis shows that in neutral $Zn(B_{12}H_{12})$, Zn s–p orbital has a significant contribution at LUMO, and HOMO is due to the $B_{12}H_{12}$ cluster. On the other hand, in the anion, there is a significant contribution from Zn s–p orbital at HOMO. This increase in the density of states around HOMO for Zn indicates that the added electron resides on the Zn orbital, which is consistent with the NBO charge analysis shown in Fig. S2(a).† In the anionic $Al(BeB_{11}H_{12})$, Al s–p orbital has a significant contribution at HOMO, which is negligible in the neutral. This also suggests that the added electron mainly resides on Al, consistent with the NBO charge analysis in Fig. S2(b).†

Fig. 3 shows the 2D and 3D charge density difference (CDD) for $Zn(B_{12}H_{12})$ and $Al(BeB_{11}H_{12})$ clusters. The regions where electrons are accumulated and depleted are represented by yellow and blue colors, respectively, in the 3D CDD plot. In $Zn(B_{12}H_{12})$, we observe positive charge density along the Zn–H bond. At the same time, the surrounding Zn regions show that there is an apparent charge depletion, indicating charge transfer from Zn during the formation of the $Zn(B_{12}H_{12})$ complex. These observations suggest that the bonding of Zn with the cluster is primarily ionic. By analyzing the CDD for $Al(BeB_{11}H_{12})$, a similar conclusion can be made.

To further understand the nature of bonding of the metal atoms in these clusters, we performed Bader's quantum theory of atoms in molecules (QTAIM) analysis. In addition, we calculated the Laplacian and gradient of the electron density. The existence of the bonds between atoms is characterized by the

 This journal is © The Royal Society of Chemistry 2022

Open Access Article. Published on 23 December 2021. Downloaded on 1/20/2026 12:19:44 PM.
This article is licensed under a Creative Commons Attribution-NonCommercial 3.0 Unported Licence.

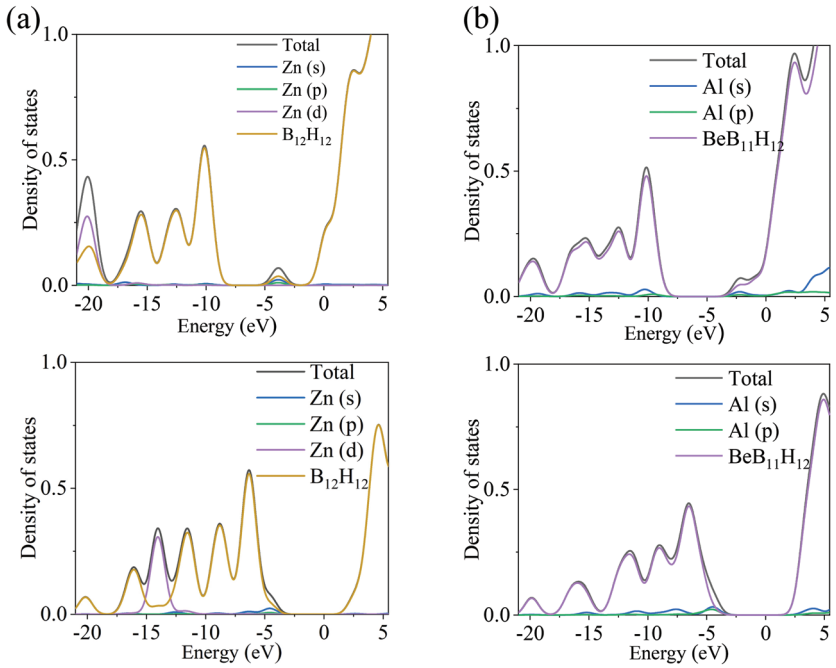

Fig. 2 Partial density of states showing various orbital contributions in (a) $Zn(B_{12}H_{12})$ neutral (top) and anion (bottom), (b) $Al(BeB_{11}H_{12})$ neutral (top) and anion (bottom). In neutral and anionic $Zn(B_{12}H_{12})$ HOMO lies at −9.86, −4.58 eV; while in $Al(BeB_{11}H1_2)$ it is at −9.36, −4.49 eV respectively.

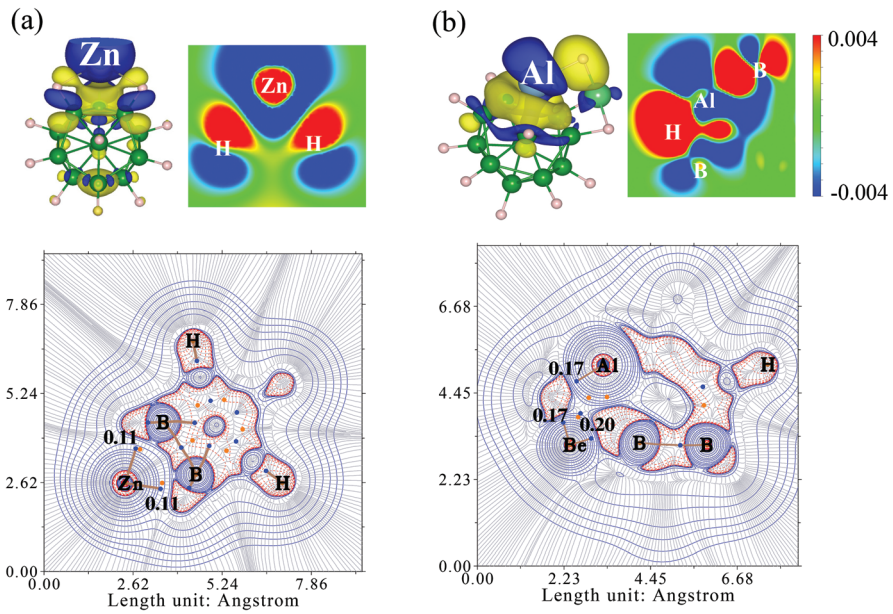

Fig. 3 Calculated CDD (top) and contour map of the Laplacian of electron density with BCPs (bottom) in (a) $Zn(B_{12}H_{12})$, and (b) $Al(BeB_{11}H_{12})$; 3D, 2D CDD plots along Zn–H and Al–H bond are shown. In the contour plot (bottom panel), blue and orange dots represent the bond and ring critical points, respectively. Red and blue lines indicate the regions where the charge is concentrated and depleted. The gradient of the electron density is presented in the background. The numerical values of the Laplacian of electron density (in atomic units) are presented at corresponding BCPs.

bond critical points (BCPs) obtained using QTAIM analysis. Besides, the molecular graph provides additional information on the bonding and the existing bond paths when the metal atom is bonded to the cluster. The Laplacian of the electron density expresses quantitively the characteristic of the interaction at the BCPs between interacting atoms. A negative value of the Laplacian ($\nabla^2\rho(r) < 0$) at BCP corresponds to the covalent nature of the bond, while the positive value of the Laplacian ($\nabla^2\rho(r) > 0$) shows the non-covalent (ionic/polar) nature of the bond. The contour map of the Laplacian of the electron

Open Access Article. Published on 23 December 2021. Downloaded on 1/20/2026 12:19:44 PM.
This article is licensed under a Creative Commons Attribution-NonCommercial 3.0 Unported Licence.

density indicates charge concentration ($\nabla^2\rho(r) < 0$) or charge depletion ($\nabla^2\rho(r) > 0$) regions. The contour maps of the Laplacian of electron density with BCPs highlighting the Zn–H and Zn–B interaction in $Zn(B_{12}H_{12})$ and the interaction of Be and Al with the cluster in $Al(BeB_{11}H_{12})$ are shown in Fig. 3. In $Zn(B_{12}H_{12})$, a BCP is observed between Zn and H. The positive values of the Laplacian at BCP, namely 0.11, indicate mostly the ionic nature of bonding as observed from the CDD plot. A similar observation is made in $Al(BeB_{11}H_{12})$, with the Al–H bond having a positive value of the Laplacian. A molecular graph representing the QTAIM topology of the critical points and possible bond paths for these clusters are shown in Fig. S3.†

We have calculated the binding energy of the neutral and anion by using the formula: $E_b^0 = E(M) + E(B_{12}H_{12}) - E(MB_{12}H_{12})$ and $E_b^- = E(M) + E(B_{12}H_{12}^-) - E(MB_{12}H_{12}^-)$, where M is the metal atom. The binding energy of Zn in neutral $Zn(B_{12}H_{12})$, is 2.16 eV, while in the anion it is 1.75 eV. The relative strength of bonding in the neutral and the anionic cluster can be qualitatively understood by using the bond distances between the metal atom and the cluster (H, B) atoms. The decrease in BE in the anion is attributed to the increase in bond length between Zn–(H/B) in Fig. 1(a and b).

B. Metallo-boranes with one extra electron than needed for electron shell closure: $Zn(B_{12}H_{11})$, $Zn(CB_{11}H_{12})$, and $Al(B_{12}H_{12})$

Here, we consider three metallo-borane clusters $Zn(B_{12}H_{11})$, $Zn(CB_{11}H_{12})$, and $Al(B_{12}H_{12})$. Note that removing one H atom from $B_{12}H_{12}$ leaves it as a $B_{12}H_{11}$ cluster that requires only one extra electron to satisfy the electron shell closure rule. With Zn contributing two electrons to the boron cage, $Zn(B_{12}H_{11})$ has one electron more than required for electron shell closure. Similarly, replacing one B atom with a C atom adds an extra electron to the core. Thus, $Zn(CB_{11}H_{12})$ is isoelectronic with $Zn(B_{12}H_{11})$ and has one electron more than needed electron shell closure. Similarly, Al being trivalent, $Al(B_{12}H_{12})$ also has one extra electron than needed for shell closure. Due to this extra electron, initially, we expected these clusters to mimic the chemistry of alkali atoms and, due to their large size, to behave as superalkalis. This is consistent with our previous work[34] where we had demonstrated that $Li_3(B_{12}H_{12})$, with a VIE of 3.24 eV, behaves as a superalkali. In Table 1, we present the EA and VIE of $Zn(B_{12}H_{11})$, $Zn(CB_{11}H_{12})$, and $Al(B_{12}H_{12})$. Contrary to our expectation, these clusters have VIEs higher than that of Na, which is 5.14 eV, and do not behave as superalkalis. Instead, the EAs of these clusters is higher than that of Cl, making these superhalogens. In the following, we discuss the reasons for this unusual behavior.

We begin with the equilibrium geometries of neutral $Zn(B_{12}H_{11})$, $Al(B_{12}H_{12})$, and $Zn(CB_{11}H_{12})$ clusters as shown in Fig. 4(a, b and c), respectively. Note that even when we remove one H atom or substitute one of the B atoms in the cage with C, the resulting cage structure remains intact. In $Zn(B_{12}H_{11})$, Zn is at a distance of 2.24 Å from two H atoms and 1.98 Å from the third H atom. In comparison, the three nearest B atoms are at distances of 2.30, 2.42, and 2.42 Å from Zn. In $Zn(CB_{11}H_{12})$, the three nearest H atoms lie at distances of 2.05, 2.14, and 2.14 Å from Zn, while two B atoms are at 2.38 Å, and the third one is at 2.35 Å from Zn. In $Al(B_{12}H_{12})$, Al is at a distance of 1.88 Å from the three closest H atoms, while it is at a distance of 2.13 Å from the three B atoms.

The geometries for anionic $Zn(B_{12}H_{11})$, $Al(B_{12}H_{12})$, and $Zn(CB_{11}H_{12})$ clusters are shown in Fig. 4(d, e and f), respectively. In anionic $Zn(B_{12}H_{11})$, the Zn–H distances increase from its neutral and lie in the range 2.97–3.14 Å (the range in neutral is 1.98–2.24 Å) and Zn–B distance lies in the range 3.58–3.64 Å

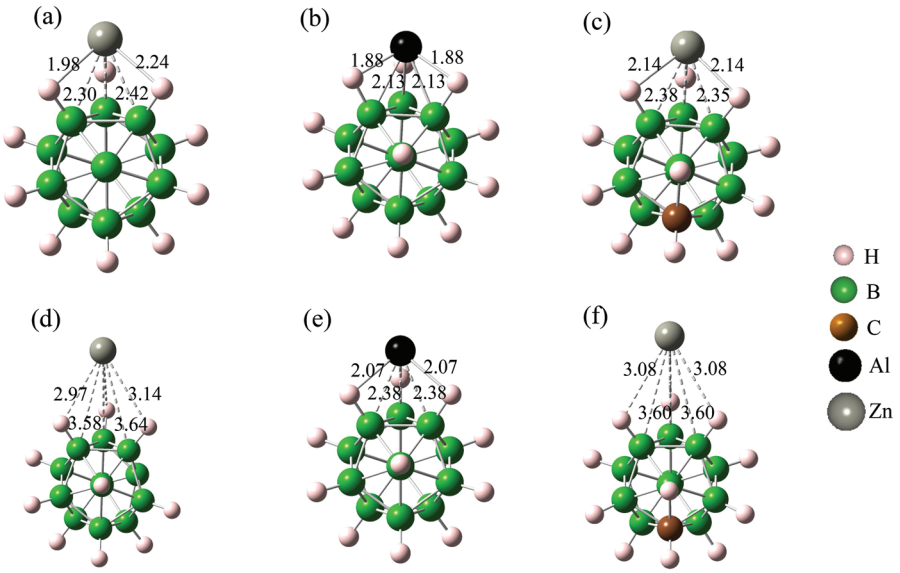

Fig. 4 Optimized geometries of neutral (a) $Zn(B_{12}H_{11})$, (b) $Al(B_{12}H_{12})$, (c) $Zn(CB_{11}H_{12})$, and anionic (d) $Zn(B_{12}H_{11})$, (e) $Al(B_{12}H_{12})$, and (f) $Zn(CB_{11}H_{12})$ clusters. The bond length (in Å) between the adatom and the nearest atom in the cluster is presented.

Open Access Article. Published on 23 December 2021. Downloaded on 1/20/2026 12:19:44 PM.
This article is licensed under a Creative Commons Attribution-NonCommercial 3.0 Unported Licence.

(for neutral it lies in the range 2.30–2.42 Å). This indicates that the addition of an electron weakens the Zn bonding with the cluster. At the same time, the bonding of H with the cage becomes stronger, which is indicated by a decrease in the B–H bond length in the anion. In the neutral $Zn(B_{12}H_{11})$, B–H bond length ranges from 1.19 to 1.23 Å, while in the anion, it is 1.19 Å. As observed previously, in the anion, the average bond length between the adatom and the cluster atom is increased, despite geometric distortion.

To understand the reason for the superhalogen behavior of these clusters, which should be behaving like superalkalis, we examine the charge distribution. In neutral $Zn(B_{12}H_{11})$, the charge on Zn is +0.87*e*, while that on the naked B on the cage is +0.68*e*. When an electron is added, it neutralizes the positive charge on the Zn atom, as shown by the natural distribution values (Zn has a null charge in anion) in Fig. S4(a).† Note that there is very little change in the charge on the naked B atom (+0.64*e* in the anion).

In $Al(B_{12}H_{12})$, the difference in bond length and the distribution of additional electrons follow the same trend as in $Zn(B_{12}H_{11})$. Al–H bond length increases from 1.88 Å in the neutral to 2.07 Å in the anion, indicating a weakening of the Al bonding (see Fig. 4(b and e)). Besides, the Al binding energies of 4.93 eV in the neutral and 4.65 eV in the anion are consistent with the differences in Al–(H/B) bond distances in their neutral and anionic states in Fig. 4(b and e). Similar reasoning holds for the $Zn(CB_{11}H_{12})$ cluster (Fig. 4(c and f)). Natural charge distributions in neutral and anionic $Al(B_{12}H_{12})$ and $Zn(CB_{11}H_{12})$ in Fig. S4(b) and (c)† indicate a decrease in the charge on Al and Zn in the anionic cluster compared to that in the neutral. This suggests that the added electron mainly resides on the metal atom rather than being distributed on the borane cage.

We now analyze the electronic structure and nature of bonding in these clusters. Fig. 5 shows the projected density of states of the neutral and anionic $Zn(B_{12}H_{11})$, $Zn(CB_{11}H_{12})$, and $Al(B_{12}H_{12})$ clusters. In the neutral and anionic $Zn(B_{12}H_{11})$, Zn-s orbital has a significant contribution at HOMO. In the anionic $Al(B_{12}H_{12})$ and $Zn(CB_{11}H_{12})$ clusters, the HOMO is constituted mostly of the Al-s and Zn-s orbitals, respectively. Besides these observations, the NBO analysis presented in Fig. S4† indicates that the additional electron in these clusters mainly resides on the metal adatom.

The CDD plots for these clusters in 2D and 3D are shown in Fig. 6. Note that there is an apparent deficiency in the charge around the region surrounding Zn and Al, indicating charge transfer from these metal atoms during the formation of the respective complexes.

The contour maps of the Laplacian of electron density with bond critical points highlighting the interaction of the adatom (Zn, Al) with the cluster atoms (H, B) in $Zn(B_{12}H_{11})$, $Zn(CB_{11}H_{12})$, and $Al(B_{12}H_{12})$ are shown in Fig. 6, while the corresponding molecular graph representing the QTAIM topology of the critical points and possible bond paths are shown in Fig. S5.† In $Zn(B_{12}H_{11})$, BCP is observed along the shortest Zn–H bond, which is further verified by the existence of the bond path along one H atom in Fig. S5(a).† The location of the BCP at the positive contour of the Laplacian ($\nabla^2\rho(r)$ = 0.10) indicates the primarily ionic nature of the Zn–H interaction. No BCP is observed between Zn–B in $Zn(B_{12}H_{11})$, which is reflected by the characteristic Zn–B bond length in Fig. 4. In $Al(B_{12}H_{12})$, BCP is observed along the axis passing through the centroid of the triangle formed by three B atoms of the *closo*-borane ring. The location of the BCP at the positive contour of Laplacian ($\nabla^2\rho(r)$ = 0.08) indicates polar (very weak ionic, but no covalent) interaction of Al in $Al(B_{12}H_{12})$. Since no BCP is observed along Al–H in $Al(B_{12}H_{12})$, Al–H interactions are implicitly influenced by the electron densities along with Al–H and B–H atoms.

The bonding of Zn in $Zn(CB_{11}H_{12})$ is similar to that in $Zn(B_{12}H_{11})$. BCP is observed along the shortest Zn–H bond (namely 2.05 Å) in $Zn(CB_{11}H_{12})$, as shown in Fig. 6(c).

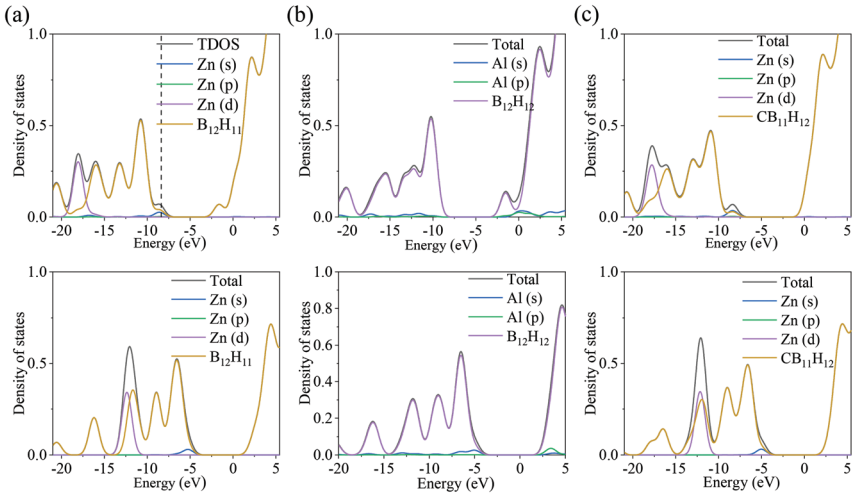

Fig. 5 Partial density of states of neutral (top) and anion (bottom) state of (a) $Zn(B_{12}H_{11})$, (b) $Al(B_{12}H_{12})$, and (c) $Zn(CB_{11}H_{12})$. HOMO lies at −8.59, −9.87, and −8.37 eV in the neutral $ZnB_{12}H_{11}$, $AlB_{12}H_{12}$, $Zn(CB_{11}H_{12})$ and at −5.22, −5.0, and −5.02 eV in their anions.

Open Access Article. Published on 23 December 2021. Downloaded on 1/20/2026 12:19:44 PM.
This article is licensed under a Creative Commons Attribution-NonCommercial 3.0 Unported Licence.

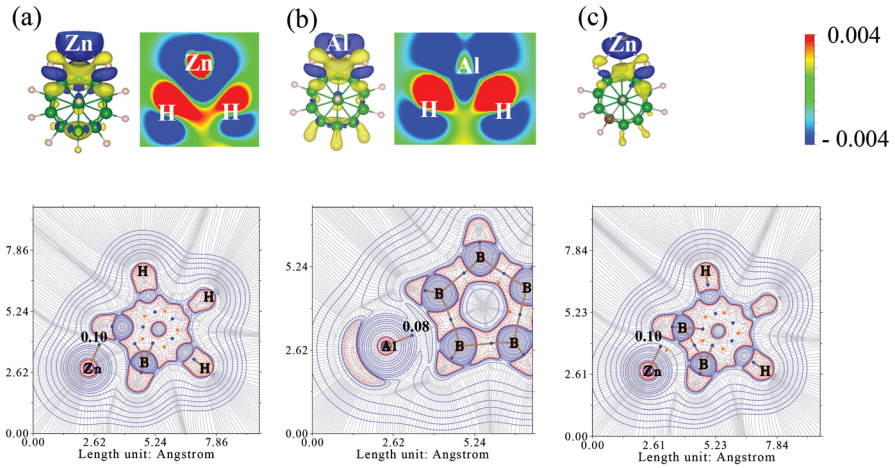

Fig. 6 Calculated CDD (top) and Contour map of the Laplacian of electron density with BCPs (bottom) in (a) $Zn(B_{12}H_{11})$, (b) $Al(B_{12}H_{12})$, and (c) $Zn(CB_{11}H_{12})$. 3D, 2D CDD plots along Zn–H and Al–H bonds are shown. In the contour plot (bottom panel), the numerical values of the Laplacian of electron density (in atomic units) are presented at corresponding BCPs.

C. Metallo-borane with one electron less than required for the electronic shell closure: $Zn(BeB_{11}H_{12})$ and $Li(B_{12}H_{12})$

Here, we consider $Zn(BeB_{11}H_{12})$ and $Li(B_{12}H_{12})$ clusters as an example. Replacing one B atom with a Be atom requires three electrons to satisfy the electron shell closure requirement of $BeB_{11}H_{12}$. As Zn can only provide two electrons, $Zn(BeB_{11}H_{12})$ cluster requires an extra electron to satisfy its shell closure. Similarly, $Li(B_{12}H_{12})$ requires an extra electron to satisfy the Wade–Mingos rule. The extra electron has the option to distribute over the boron cage as would be the case with conventional superhalogens. On the other hand, the extra electron could also reside on the doped metal ion as it remains in a positively charged state. Either way, these clusters should have electron affinities larger than that of Cl. To see which mechanism is dominant, we calculated the geometries of neutral and anionic $Zn(BeB_{11}H_{12})$ and $Li(B_{12}H_{12})$ clusters. These are given in Fig. 7 (a, b, c and d). In $Zn(BeB_{11}H_{12})$, Zn and Be are both at the edge of the square formed by four B atoms. H atoms are displaced from their original positions as well. One H atom forms a triangle with Zn and Be with sides 1.46, 1.78, and 2.24 Å. The shortest Zn–H distance is 1.78 Å, two B atoms are at a distance of 2.21 Å from Zn, while the third one is at 2.13 Å. The two closest H atoms are equidistant from Be, namely at 1.61 Å, and the third H is at 1.46 Å. Also, two B atoms are equidistant from Be, namely at 1.81 Å. Compared to other B–H bond lengths, the one on which Be is bonded gets elongated, namely 1.27 Å, compared to 1.19 Å. This indicates a weakening of the B–H bond near the Be adsorbed site. In the neutral $Li(B_{12}H_{12})$, the three shortest Li–H distances are 2.02 Å and the shortest Li–B distance is 2.25 Å; while in the anion, these distances are at 1.95 Å and 2.17 Å respectively.

The natural charge distributions in $Zn(BeB_{11}H_{12})$ and $Li(B_{12}H_{12})$ are shown in Fig. S6.† In the anionic state, a slight change in the charge on the Zn (+1.15*e* in neutral *vs.* +0.94*e* in the anion) and Be (+1.57*e* in neutral *vs.* +1.52*e* in the anion) in $Zn(BeB_{11}H_{12})$, and on the Li (+0.97*e* in neutral *vs.* +0.95*e* in the anion) atom in $Li(B_{12}H_{12})$ is observed. This indicates that the additional electron mainly resides on the boron cage. The projected density of states for the neutral and anionic states of $Zn(BeB_{11}H_{12})$ and $Li(B_{12}H_{12})$ are shown in Fig. 8. In both clusters, in their neutral and anionic state, the adatom has no noticeable contribution at HOMO and LUMO. Besides, in both clusters, the CDD plot in Fig. 9 shows an apparent deficiency in the charge around the surrounding region of metal atoms during the formation of the complex. Unlike other clusters we studied, the higher value of the EA, namely, 3.67 eV in $Zn(BeB_{11}H_{12})$ and 4.85 eV in $Li(B_{12}H_{12})$, is due to the delocalization of the extra electron over the boron atoms forming the cage.

The contour map of the Laplacian highlighting the Zn and Be interaction with cluster atoms in $Zn(BeB_{11}H_{12})$ and Li interaction with cluster atoms in $Li(B_{12}H_{12})$ is shown in Fig. 9. In $Zn(BeB_{11}H_{12})$, BCP is observed between Zn–B, Zn–H, and Be–H. The existence of BCP between Zn–B is along the shortest Zn–B distance, namely 2.13 Å, while no BCP is observed along Zn–Be. While in $Li(B_{12}H_{12})$, BCP is observed along the axis passing through the centroid of the triangle formed by three B atoms of the *closo*-borane ring. The existence of the bond path between the metal atoms (Zn, Be, and Li) to the cluster atoms in Fig. S7† further explains the bonding in these clusters. As before, the nature of Zn and Li bonding can be further understood by the corresponding Laplacian values at the BCP, in Fig. 9.

4. Limitations and future prospects

Now, we examine the limitations in the design of this new class of superhalogens and explore the future prospects of the metallo-borane class of superhalogens. First, the limitations:

 This journal is © The Royal Society of Chemistry 2022

Open Access Article. Published on 23 December 2021. Downloaded on 1/20/2026 12:19:44 PM.
This article is licensed under a Creative Commons Attribution-NonCommercial 3.0 Unported Licence.

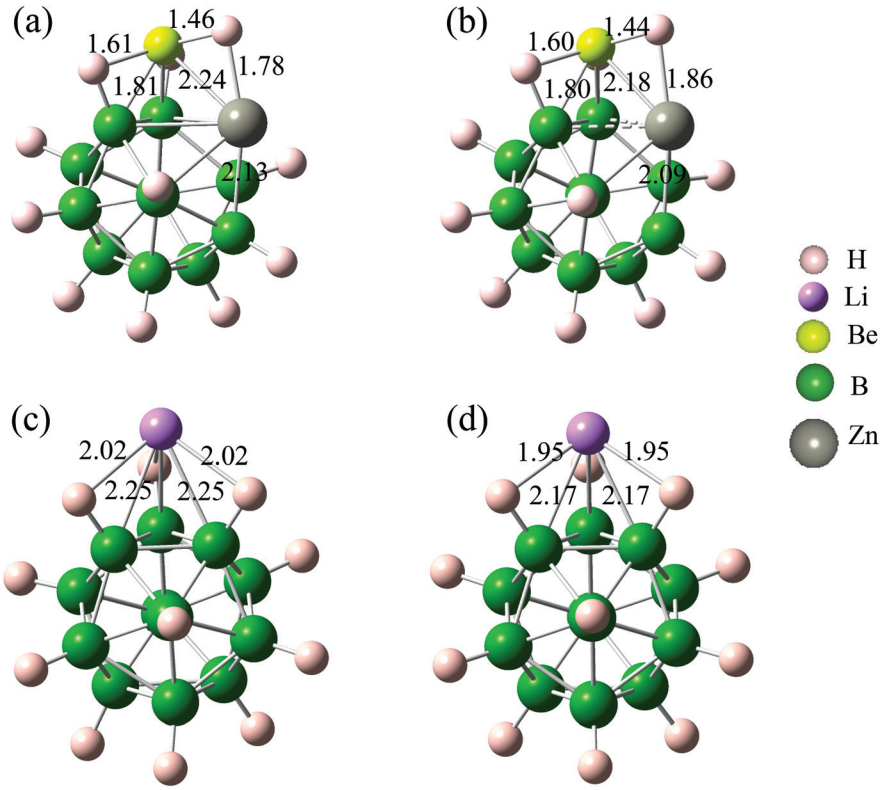

Fig. 7 Optimized geometries of (a) neutral, (b) anionic $Zn(BeB_{11}H_{12})$ and (c) neutral, (d) anionic $Li(B_{12}H_{12})$. The bond length (in Å) between the adatom and the nearest atom in the cluster is presented. The color coding for the atoms is the same as in Fig. 1, except the atom in magenta color (in c and d) represents the lithium atom.

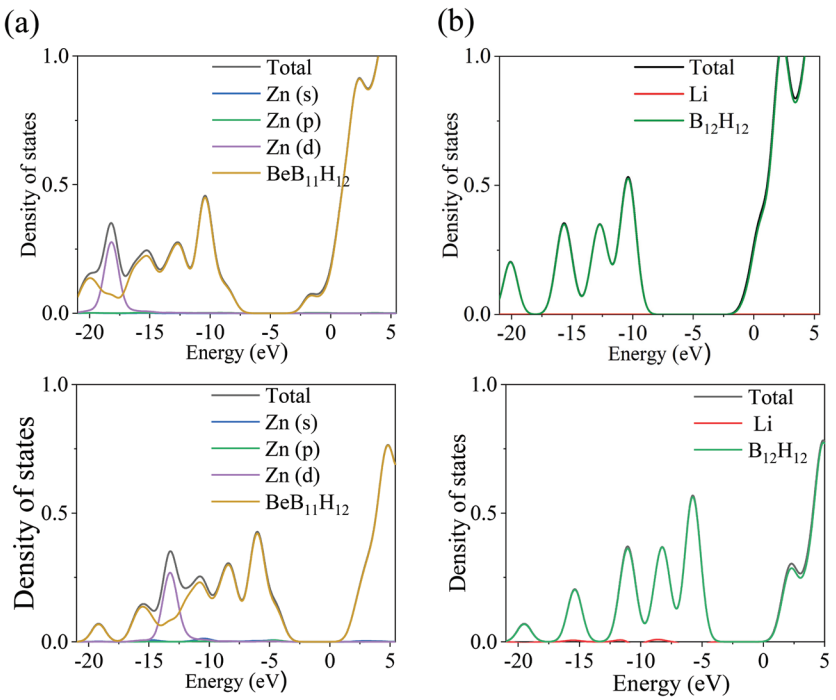

Fig. 8 Partial density of states of neutral (top) and anion (bottom) in (a) $Zn(BeB_{11}H_{12})$, and (b) $LiB_{12}H_{12}$. In $Zn(BeB_{11}H_{12})$, HOMO lies at −8.43 eV in the neutral and at −4.28 eV in the anion. In $LiB_{12}H_{12}$, HOMO lies at −9.49 eV in the neutral and at −5.41 eV in the anion.

Open Access Article. Published on 23 December 2021. Downloaded on 1/20/2026 12:19:44 PM.
This article is licensed under a Creative Commons Attribution-NonCommercial 3.0 Unported Licence.

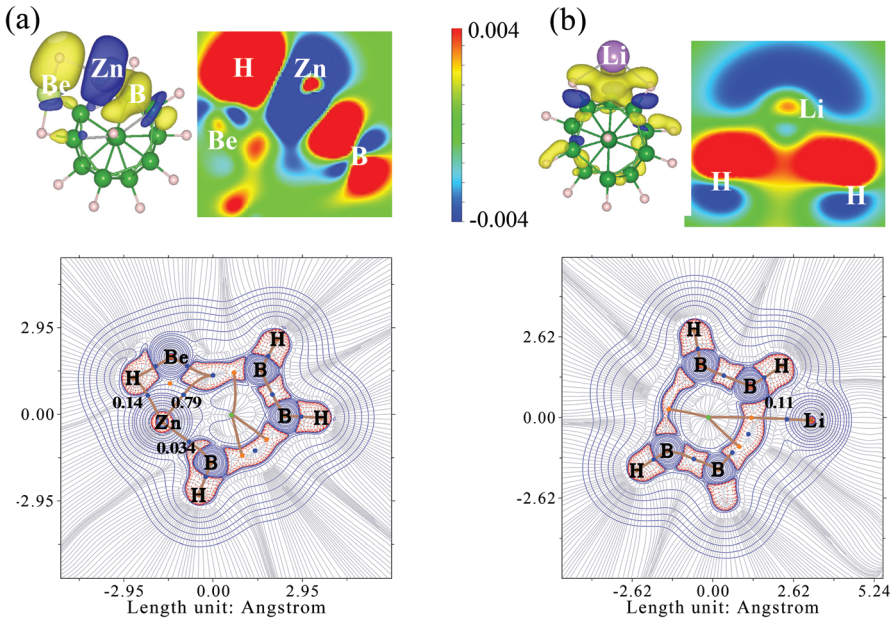

Fig. 9 Calculated CDD in 3D and 2D (top) and contour map of the Laplacian of electron density with BCPs (bottom) in (a) $Zn(BeB_{11}H_{12})$ and (b) $Li(B_{12}H_{12})$. The CDD plot shows the accumulation and depletion of charge along the Zn–H, Be–H in (a), and Li–H bond in (b). The contour map of the Laplacian of electron density shows the interaction between different atoms. The numerical values of the Laplacian of electron density (in atomic units) are presented at corresponding BCPs.

can any metal adsorbed onto a borane-based cluster produce a superhalogen? For this, we focus on $Li_2(B_{12}H_{12})$, which is a closed shell cluster, and $Li_3(B_{12}H_{12})$, which has one electron more than needed for shell closure. Being a closed shell species, $Li_2(B_{12}H_{12})$, as expected, is neither a superhalogen nor a superalkali (EA = 0.25 eV and VIE = 9.38 eV). Similarly, as expected, $Li_3(B_{12}H_{12})$ is a superalkali (EA = 0.22 eV and VIE = 3.24 eV), but not a superhalogen. In addition, the computed EA for $Na_2(B_{12}H_{12})$ is 0.39 eV. This shows that even if the alkali metal atoms donate electrons to the boron cage, the resulting clusters are not superhalogens. One possible reason could be that the ionization energies of the added Li and Na atoms, namely 5.39 and 5.14 eV, respectively, are small. Thus, when the additional electron partially neutralizes the charge on Li and Na, the energy gain is small, leading to the small EA in $Li_2B_{12}H_{12}$ and $Na_2B_{12}H_{12}$.

Moving further, we studied the importance of *closo*-boranes in the observed superhalogen behavior. Note that O and S require two electrons for shell closure as $B_{12}H_{12}$ does. Do ZnO and ZnS behave as superhalogens? We computed the EAs for ZnO and ZnS, which are 2.30 eV for the former and 2.39 eV for the later. Thus, these are not superhalogens. We conclude that there is a limitation to this new class of superhalogens. Not all metal compounds will be superhalogens just because the metal atom donates their electrons during the bonding. Similarly, chalcogens cannot substitute $B_{12}H_{12}$ in the formation of superhalogens.

Thus, the choice of the negative ion components and high ionization energy of the metal atoms is important in the design of more unconventional superhalogens. For example, H in the $B_{12}H_{12}$ can be replaced by more electronegative ligands such as halogens (F, Cl) and superhalogens (CN, BO). Previous studies have shown that the electron affinities of $B_{12}X_{12}$ can be substantially increased when X is a halogen or a superhalogen. It will be interesting to study the electron affinities of $Zn(B_{12}X_{12})$ (X = F, Cl, Br, CN, BO) species. Another promising study is to use transition metal (TM) elements other than Zn, noting that TM elements not only have large ionization energies but also, they carry magnetic moments. For example, could $TM(B_{12}X_{12})$ be a magnetic superhalogen?

5. Conclusion

Using density functional theory with a long range corrected hybrid exchange–correlation functional (ωB97XD) and the 6-311+g(d,p) basis set, we have shown that a new class of superhalogens, called metallo-boranes, can be designed. A particularly interesting example is $Zn(B_{12}H_{12})$. Note that the electron affinity of the Zn atom is −0.60 eV; this is due to the fact that Zn has a closed $4s^2$ shell. $Zn(B_{12}H_{12})$ also has a closed electronic shell with a HOMO–LUMO gap of 6.0 eV. Thus, $Zn(B_{12}H_{12})$ should mimic the chemistry of noble gas atoms, and its electron affinity should be minimal. Yet, its electron affinity is 4.30 eV, making it a superhalogen. Among the studied metallo-boranes (*i.e.*, clusters with closed shell and one extra electron than required for the electron shell closure), $Al(B_{12}H_{12})$ has the highest EA, namely 4.43 eV, and $Al(BeB_{11}H_{12})$ has the lowest, namely 3.61 eV. The basic difference between the traditional superhalogens and these metallo-

 This journal is © The Royal Society of Chemistry 2022

Open Access Article. Published on 23 December 2021. Downloaded on 1/20/2026 12:19:44 PM.
This article is licensed under a Creative Commons Attribution-NonCommercial 3.0 Unported Licence.

boranes is the underlying principle governing superhalogen behavior. Unlike traditional superhalogens (with composition MX_{k+1}) in which the added electron is distributed over a large phase space provided by the halogen atoms, in the metallo-boranes, the added electron mainly resides on the doped metal site to neutralize its positive charge resulting from charge transfer. However, not all metal atoms bound to the $B_{12}H_{12}$ cage can lead to superhalogens; only those that have high ionization energy can. More interestingly, we found that, unlike the conventional superhalogens, the metallo-borane class of superhalogens defy the electron shell closure rule, thereby expanding the scope for their design and synthesis. In addition, the discovery of this new class of superhalogens opens the door for the design of magnetic superhalogens by doping transition metal atoms. It will be interesting to study if materials synthesized with these magnetic superhalogens could potentially produce ferromagnetic semiconductors. The prospects of designing and synthesizing new materials with tailored properties can bring a new dimension to the superhalogen research.

Conflicts of interest

There are no conflicts to declare.

Acknowledgements

This work is partially supported by the U.S. Department of Energy, Office of Basic Energy Sciences, Division of Materials Sciences and Engineering under Award DE-FG02-96ER45579. Resources of the National Energy Research Scientific Computing Center supported by the Office of Science of the U.S. Department of Energy under Contract no. DE-AC02-05CH11231 is also acknowledged.

References

1 P. Jena and Q. Sun, Super Atomic Clusters: Design Rules and Potential for Building Blocks of Materials, *Chem. Rev.*, 2018, **118**, 5755–5870.
2 G. L. Gutsev and A. I. Boldyrev, DVM-X_α calculations on the ionization potentials of MX_{k+1}^- complex anions and the electron affinities of MX_{k+1} "superhalogens", *Chem. Phys.*, 1981, **56**, 277–283.
3 G. L. Gutsev and A. I. Boldyrev, DVM X_α calculations on the electronic structure of "superalkali" cations, *Chem. Phys. Lett.*, 1982, **92**, 262–266.
4 S. Giri, S. Behera and P. Jena, Superalkalis and Superhalogens As Building Blocks of Supersalts, *J. Phys. Chem. A*, 2014, **118**, 638–645.
5 M. Willis, M. Götz, A. K. Kandalam, G. F. Ganteför and P. Jena, Hyperhalogens: Discovery of a New Class of Highly Electronegative Species, *Angew. Chem., Int. Ed.*, 2010, **49**, 8966–8970.
6 P. Jena, Materials for Hydrogen Storage: Past, Present, and Future, *J. Phys. Chem. Lett.*, 2011, **2**, 206–211.
7 S. Giri, S. Behera and P. Jena, Superhalogens as building blocks of halogen-free electrolytes in lithium-ion batteries., *Angew. Chem., Int. Ed.*, 2014, **53**, 13916–13919.
8 H. Fang and P. Jena, Super-ion inspired colorful hybrid perovskite solar cells, *J. Mater. Chem. A*, 2016, **4**, 4728–4737.
9 H. Fang and P. Jena, Sodium Superionic Conductors Based on Clusters, *ACS Appl. Mater. Interfaces*, 2019, **11**, 963–972.
10 Y. Gao, M. Wu and P. Jena, A family of ionic supersalts with covalent-like directionality and unconventional multiferroicity, *Nat. Commun.*, 2021, **12**, 1331.
11 C. Sikorska, S. Smuczyńska, P. Skurski and I. Anusiewicz, BX_4^- and AlX_4^- Superhalogen Anions (X=F, Cl, Br): An ab Initio Study, *Inorg. Chem.*, 2008, **47**, 7348–7354.
12 I. Anusiewicz, M. Sobczyk, I. Dąbkowska and P. Skurski, An ab initio study on MgX_3^- and CaX_3^- superhalogen anions (X=F, Cl, Br), *Chem. Phys.*, 2003, **291**, 171–180.
13 A. N. Alexandrova, A. I. Boldyrev, Y.-J. Fu, X. Yang, X.-B. Wang and L.-S. Wang, Structure of the $Na_xCl_{x+1}^-$ (x=1–4) clusters via ab initio genetic algorithm and photoelectron spectroscopy, *J. Chem. Phys.*, 2004, **121**, 5709–5719.
14 D. F. Hunt, G. C. Stafford, F. W. Crow and J. W. Russell, Pulsed positive negative ion chemical ionization mass spectrometry, *Anal. Chem.*, 1976, **48**, 2098–2104.
15 B. M. Elliott, E. Koyle, A. I. Boldyrev, X.-B. Wang and L.-S. Wang, MX_3^- Superhalogens (M=Be, Mg, Ca; X=Cl, Br): A Photoelectron Spectroscopic and ab Initio Theoretical Study, *J. Phys. Chem. A*, 2005, **109**, 11560–11567.
16 I. Langmuir, The arrangement of electrons in atoms and molecules., *J. Am. Chem. Soc.*, 1919, **41**, 868–934.
17 I. Langmuir, Types of valence, *Science*, 1921, **54**, 59–67.
18 H.-J. Zhai, J. Li and L.-S. Wang, Icosahedral gold cage clusters: $M@Au_{12}^-$ (M=V, Nb, and Ta), *J. Chem. Phys.*, 2004, **121**, 8369–8374.
19 S. Freza and P. Skurski, Enormously large (approaching 14eV!) electron binding energies of $[H_nF_{n+1}]^-$ (n=1–5, 7, 9, 12) anions, *Chem. Phys. Lett.*, 2010, **487**, 19–23.
20 A. I. Boldyrev and J. Simons, Vertical and adiabatical ionization potentials of MH^-_{K+1} anions. Ab initio study of the structure and stability of hypervalent MH_{k+1} molecules, *J. Chem. Phys.*, 1993, **99**, 4628–4637.
21 K. Wade, The structural significance of the number of skeletal bonding electron-pairs in carboranes the higher boranes and borane anions and various transition-metal carbonyl cluster compounds, *J. Chem. Soc. D*, 1971, 792–793.
22 E. Hückel, Zur Quantentheorie der Doppelbindung, *Eur. Phys. J. A*, 1930, **60**, 423–456.
23 E. Hückel, Quantentheoretische Beiträge zum Benzolproblem, *Z. Phys.*, 1931, **70**, 204–286.
24 B. Pathak, D. Samanta, R. Ahuja and P. Jena, Borane derivatives: a new class of super- and hyperhalogens, *ChemPhysChem*, 2011, **12**, 2423–2428.

Open Access Article. Published on 23 December 2021. Downloaded on 1/20/2026 12:19:44 PM.
This article is licensed under a Creative Commons Attribution-NonCommercial 3.0 Unported Licence.

25 H. Zhao, J. Zhou and P. Jena, Stability of $B_{12}(CN)_{12}^{2-}$: Implications for Lithium and Magnesium Ion Batteries, *Angew. Chem., Int. Ed.*, 2016, **55**, 3704–3708.
26 B. Z. Child, S. Giri, S. Gronert and P. Jena, Aromatic Superhalogens, *Chem. – Eur. J.*, 2014, **20**, 4736–4745.
27 C. Paduani, M. M. Wu, M. Willis and P. Jena, Theoretical Study of the Stability and Electronic Structure of Al $(BH_4)_{n=1\rightarrow4}$ and $Al(BF_4)_{n=1\rightarrow4}$ and Their Hyperhalogen Behavior, *J. Phys. Chem. A*, 2011, **115**, 10237–10243.
28 H. Fang and P. Jena, Stable Tetra- and Penta-Anions in the Gas Phase, *Angew. Chem., Int. Ed.*, 2019, **58**, 11248–11252.
29 S. Li, M. Willis and P. Jena, Reaction Intermediates during the Dehydrogenation of Metal Borohydrides: A Cluster Perspective, *J. Phys. Chem. C*, 2010, **114**, 16849–16854.
30 M. L. McKee, Z.-X. Wang and P. von R. Schleyer, Ab Initio Study of the Hypercloso Boron Hydrides B_nH_n and $B_nH_n^-$. Exceptional Stability of Neutral $B_{13}H_{13}$, *J. Am. Chem. Soc.*, 2000, **122**, 4781–4793.
31 W. Kohn and L. J. Sham, Self-Consistent Equations Including Exchange and Correlation Effects, *Phys. Rev.*, 1965, **140**, A1133–A1138.
32 J.-D. Chai and M. Head-Gordon, Long-range corrected hybrid density functionals with damped atom–atom dispersion corrections, *Phys. Chem. Chem. Phys.*, 2008, **10**, 6615–6620.
33 M. J. Frisch, G. W. Trucks, H. B. Schlegel, G. E. Scuseria, M. A. Robb, J. R. Cheeseman, G. Scalmani, V. Barone, G. A. Petersson, H. Nakatsuji, X. Li, M. Caricato, A. V. Marenich, J. Bloino, B. G. Janesko, R. Gomperts, B. Mennucci, H. P. Hratchian, J. V. Ortiz, A. F. Izmaylov, J. L. Sonnenberg, D. Williams-Young, F. Ding, F. Lipparini, F. Egidi, J. Goings, B. Peng, A. Petrone, T. Henderson, D. Ranasinghe, V. G. Zakrzewski, J. Gao, N. Rega, G. Zheng, W. Liang, M. Hada, M. Ehara, K. Toyota, R. Fukuda, J. Hasegawa, M. Ishida, T. Nakajima, Y. Honda, O. Kitao, H. Nakai, T. Vreven, K. Throssell, J. A. Montgomery Jr., J. E. Peralta, F. Ogliaro, M. J. Bearpark, J. J. Heyd, E. N. Brothers, K. N. Kudin, V. N. Staroverov, T. A. Keith, R. Kobayashi, J. Normand, K. Raghavachari, A. P. Rendell, J. C. Burant, S. S. Iyengar, J. Tomasi, M. Cossi, J. M. Millam, M. Klene, C. Adamo, R. Cammi, J. W. Ochterski, R. L. Martin, K. Morokuma, O. Farkas, J. B. Foresman and D. J. Fox, *Gaussian 16 Revision B.01*, Gaussian, Inc., Wallingford CT, 2016.
34 H. R. Banjade, Deepika Deepika, S. Giri, S. Sinha, H. Fang and P. Jena, Role of Size and Composition on the Design of Superalkalis, *J. Phys. Chem. A*, 2021, **125**, 5886–5894.
35 F. Weinhold, Natural bond orbital analysis: A critical overview of relationships to alternative bonding perspectives, *J. Comput. Chem.*, 2012, **33**, 2363–2379.
36 R. F. W. Bader, *Atoms in Molecules: A Quantum Theory*, Clarendon Press, 1990.
37 R. Bader, A Bond Path: A Universal Indicator of Bonded Interactions, *J. Phys. Chem. A*, 1998, **102**, 7314–7323.
38 T. Lu and F. Chen, Multiwfn: A multifunctional wavefunction analyzer, *J. Comput. Chem.*, 2012, **33**, 580–592.
39 P. Ros and G. C. A. Schuit, Molecular Orbital Calculations on Copper Chloride Complexes, *Theor. Chim. Acta*, 1966, **4**, 1–12.
40 J. A. Wunderlich and W. N. Lipscomb, STRUCTURE OF $B_{12}H_{12}^{-2}$ ION, *J. Am. Chem. Soc.*, 1960, **82**, 4427–4428.
41 T. Zhao, J. Zhou, Q. Wang and P. Jena, Colossal Stability of Gas-Phase Trianions: Super-Pnictogens, *Angew. Chem., Int. Ed.*, 2017, **56**, 13421–13425.

 This journal is © The Royal Society of Chemistry 2022